Published May 13, 2013

Autophagosomal Syntaxin17-dependent lysosomal degradation maintains neuronal function in *Drosophila*

Szabolcs Takáts, Péter Nagy, Ágnes Varga, Karolina Pircs, Manuéla Kárpáti, Kata Varga, Attila L. Kovács, Krisztina Hegedűs, and Gábor Juhász

Department of Anatomy, Cell and Developmental Biology, Eötvös Loránd University, H-1117 Budapest, Hungary

During autophagy, phagophores capture portions of cytoplasm and form double-membrane autophagosomes to deliver cargo for lysosomal degradation. How autophagosomes gain competence to fuse with late endosomes and lysosomes is not known. In this paper, we show that Syntaxin17 is recruited to the outer membrane of autophagosomes to mediate fusion through its interactions with ubisnap (SNAP-29) and VAMP7 in *Drosophila melanogaster*. Loss of these genes results in accumulation of autophagosomes and a block of autolysosomal degradation during basal, starvation-induced, and developmental autophagy. Viable *Syntaxin17* mutant adults show large-scale accumulation of autophagosomes in neurons, severe locomotion defects, and premature death. These mutant phenotypes cannot be rescued by neuron-specific inhibition of caspases, suggesting that caspase activation and cell death do not play a major role in brain dysfunction. Our findings reveal the molecular mechanism underlying autophagosomal fusion events and show that lysosomal degradation and recycling of sequestered autophagosome content is crucial to maintain proper functioning of the nervous system.

Introduction

Autophagy ensures degradation and recycling of intracellular material, including macromolecules and even whole organelles in eukaryotic cells. Autophagy has a role in a wide range of physiological and pathological settings, such as cellular adaptation to stress, starvation, and protection from aging, cancer, neurodegeneration, and invading pathogens (Mizushima et al., 2008). Cytoplasmic cargo sequestered into double-membrane autophagosomes by phagophore cisterns (also called isolation membranes) is transported to lysosomes for degradation and reuse to support biosynthetic and energy production pathways (Tooze and Yoshimori, 2010). Several different sources such as ER, Golgi, mitochondria, endosomes, and plasma membrane have been suggested to supply membranes for the phagophore (Axe et al., 2008; Tooze and Yoshimori, 2010). Regardless of the membrane source, all autophagosomes fuse with late endosomes and lysosomes to generate amphisomes and autolysosomes, respectively, whereas phagophores do not. Therefore, autophagosomes must gain competence for specific fusion through acquiring the required molecular machinery during their maturation process.

Vesicle fusion events are usually mediated by the action of different SNARE proteins that assemble into complexes in a combinatorial fashion. A SNARE complex contains four parallel SNARE helix bundles, supplied by a Qa SNARE and either separate Qb and Qc SNAREs or a SNAP protein that contains both Qb and Qc SNARE domains, all located on the membrane of the first vesicle, and an R SNARE anchored to the second vesicle (Hong, 2005). Yeast SNARE proteins Vam3, Vam7, Vti1, and Ykt6 have all been suggested to play a role in fusion of autophagosomes with the vacuole, the equivalent of metazoan lysosomes (Dilcher et al., 2001; Ishihara et al., 2001; Ohashi and Munro, 2010). Vam3 and Vam7 have no clear homologues in metazoa. Moreover, we and others showed that autophagosomes accumulate if formation of late endosomes is blocked in *Drosophila melanogaster* and mammals, indicating that amphisomes play a critical role in autophagosome clearance in these cells, unlike in yeast (Filimonenko et al., 2007; Rusten et al., 2007; Juhász et al., 2008). Mammalian VAMP7, VAMP8, and

Correspondence to Gábor Juhász: szmrt@elte.hu

Abbreviations used in this paper: LTR, LysoTracker red; UAS, upstream activation sequence.

Supplemental Material can be found at:
http://jcb.rupress.org/content/suppl/2013/05/08/jcb.201211160.DC1.html
Original image data can be found at:
http://jcb-dataviewer.rupress.org/jcb/browse/5905

The Rockefeller University Press $30.00
J. Cell Biol. Vol. 201 No. 4 531–539
www.jcb.org/cgi/doi/10.1083/jcb.201211160

Published May 13, 2013

Vti1b were all suggested to be involved in autophagosomal fusion events (Fader et al., 2009; Furuta et al., 2010). The accumulation of both autophagosomes and autolysosomes in *Vti1b* knockout mice indicates that this gene product is likely to function in later steps of autophagy (Atlashkin et al., 2003). Ykt6 and VAMP7 have also been implicated in the formation of phagophores in yeast and mammalian cells, respectively (Moreau et al., 2011; Nair et al., 2011).

In a screen for SNAREs involved in autophagy, we identified Syx17 (Syntaxin17, Qa), the SNAP-29 homologue ubisnap (usnp, Qbc), and VAMP7 (CG1599, R) as required for autophagosome fusion events. We showed that Syx17 is recruited to the outer membrane of autophagosomes to acquire fusion competence, and loss of *Syx17* results in neuronal dysfunction, locomotion defects, and early death of adult flies.

Results and discussion

We performed a genetic screen for SNARE proteins involved in starvation-induced autophagy, by generating GFP-marked RNAi cell clones in mCherry-Atg8a–expressing *Drosophila* fat bodies. The mCherry-Atg8a reporter is bound to phagophores and autophagosomes through a lipid anchor on its C terminus. In addition, mCherry-Atg8a attached to the inner membrane of autophagosomes is selectively transported to autolysosomes, which are prominently labeled by this reporter as a result of large-scale accumulation of the protease- and low pH–resistant mCherry tag inside lysosomes (Kimura et al., 2007). *Syx17*, *usnp*, and *VAMP7* knockdown cells showed a similar and very characteristic phenotype: small mCherry-Atg8a dots accumulated in the perinuclear region, unlike the evenly distributed, bigger, and brighter dots observed in neighboring control cells (Fig. 1, A–C and P; and Table S1 shows the results of our screen).

Depletion of *Syx17*, *usnp*, or *VAMP7* resulted in a complete block of starvation-induced punctate LysoTracker staining, a dye commonly used to label autolysosomes in *Drosophila* fat body (Fig. 1, D–F and Q). Starvation-induced LysoTracker red (LTR) staining was also impaired in *Syx17[LL]* and *VAMP7[EP]* mutant larvae that carry transposon insertions in the coding sequences of these genes 22 and 24 nucleotides downstream of the translation start site, respectively (Fig. 1, G, H, J, and R), similar to an independent RNAi line targeting *usnp* (Fig. 1, K and Q). Transgenic expression of Syx17 restored punctate LysoTracker staining in *Syx17* mutants, confirming that loss of *Syx17* caused the mutant phenotype (Fig. 1, I and R). Tandem-tagged mCherry-GFP-Atg8a is commonly used for analyzing autophagic flux (Kimura et al., 2007). This reporter is normally transported to autolysosomes where GFP is rapidly quenched, but mCherry persists in control cells (Fig. 1, L and L′). In contrast, structures positive for both GFP and mCherry accumulated in the perinuclear region of *Syx17*, *usnp*, and *VAMP7* RNAi cells, indicating a block of GFP inactivation (Fig. 1, M–O′). Developmental autophagy of the fat body at the onset of metamorphosis was also impaired in *Syx17*, *usnp*, and *VAMP7* RNAi cells (Fig. S1, A–F, M, and N).

Immunostainings revealed accumulation of endogenous Atg8a-positive dots representing autophagosomes in *Syx17*, *usnp*, and *VAMP7* loss-of-function cells compared with adjacent control fat body cells, both in starved (Fig. 2, A–C and M) and well-fed larvae (Fig. S1, G–I and O). Levels of the specific cargo p62 inversely correlate with autophagic degradation in flies and mammals (Bjørkøy et al., 2009; Pircs et al., 2012). p62 aggregates accumulated in *Syx17*, *usnp*, and *VAMP7* loss-of-function cells both in starved (Fig. 2, D–F and N) and well-fed larvae (Fig. S1, J–L and P), indicating impaired autophagic breakdown. Western blots also revealed increased p62 and autophagosome-associated, lipidated Atg8a-II levels in starved *Syx17* and *VAMP7* mutant larvae compared with controls (Fig. 2 G). Larvae expressing *usnp* RNAi in all cells showed similar accumulation of Atg8a-II and p62 (Fig. S1 Q). *Syx17* mutants are viable despite profound autophagy defects, similar to *Atg7*- and *Atg8a*-null mutants (Juhász et al., 2007; Simonsen et al., 2008). Levels of p62 and lipidated Atg8a-II also increased in well-fed *Syx17* mutant adult flies compared with controls (Fig. 2 H). Western blots using our novel polyclonal rat and guinea pig anti-Syx17 antisera detected two bands near the predicted molecular weight of this protein, both of which were missing from *Syx17* mutants (Fig. 2, G and H; and Fig. S1 R). Faint bands were visible in the independent *Syx17* transposon insertion mutant line *Syx17[WH]* (Fig. 2 G). All these results indicated that autophagosomes cannot progress to autolysosomes in the absence of *Syx17*, *usnp*, and *VAMP7*. Ultrastructural analysis indeed revealed accumulation of double-membrane autophagosomes and impaired generation of autolysosomes in starved *Syx17* mutant, *usnp* RNAi, and *VAMP7* mutant fat body cells (Fig. 2, I–L and O).

Our loss-of-function data suggested that Syx17, usnp, and VAMP7 function as part of the same SNARE complex. Human STX17 (Syntaxin17) was previously shown to bind to SNAP-29, but the significance of this interaction remained unknown (Steegmaier et al., 1998). We found that both HA-tagged usnp and VAMP7 coimmunoprecipitated with FLAG-tagged Syx17 in cultured *Drosophila* cells (Fig. 3 A). The amount of VAMP7 bound to beads increased when all three proteins were co-expressed, suggesting that Syx17 and usnp together bind more efficiently to VAMP7 than Syx17 alone (Fig. 3 A). We also produced anti-usnp antisera to detect interactions of endogenous proteins. These polyclonal rat antibodies specifically recognized endogenous usnp as a single 36-kD band, which was reduced by systemic expression of *usnp* RNAi transgenes in larvae (Fig. S1 Q). We could readily detect endogenous usnp in anti-Syx17 immunoprecipitates from lysates of adult flies (Fig. 3 B). Vice versa, endogenous Syx17 could be immunoprecipitated with anti-usnp antibodies from cultured cell lysates (Fig. 3 C).

These results established the identity of autophagosome fusion-specific SNARE complex subunits but did not reveal which ones are present on autophagosomes. As ubisnap/SNAP-29 has both Qb and Qc SNARE domains but no transmembrane domain or lipidation site, it is likely recruited to its target membrane through interaction with Syx17, a Qa SNARE. *Drosophila* Syx17 localized to the ER (Fig. S2, A and B), similar to human STX17 (Hong, 2005). *Drosophila* VAMP7 is predicted to be present in late endosomes and lysosomes (Hong, 2005). We thus reasoned that Syx17 could also localize to autophagosomes to

Published May 13, 2013

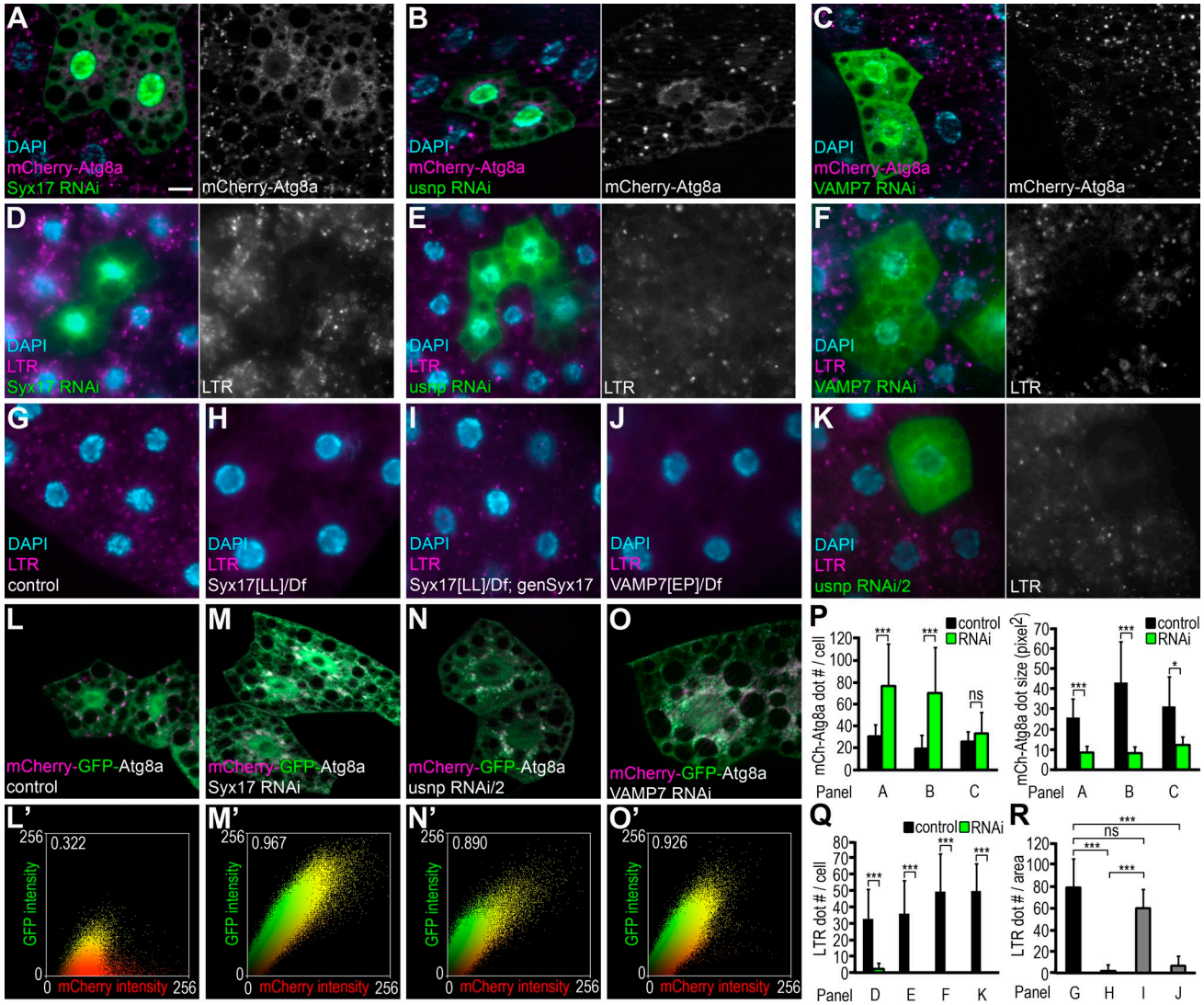

Figure 1. **Syx17, usnp, and VAMP7 are required for autophagy in *Drosophila*.** (A–C) *Syx17* (A), *usnp* (B), or *VAMP7* (C) depletion in GFP-marked fat cell clones leads to formation of numerous small, mostly perinuclear mCherry-Atg8a dots, unlike the larger, brighter, evenly distributed punctae in surrounding control cells of starved larvae. (D–F) Knockdown of *Syx17* (D), *usnp* (E), or *VAMP7* (F) in LAMP1-GFP–marked cells blocks starvation-induced punctate LysoTracker red (LTR) staining. (G–J) Starvation leads to formation of LTR dots in control larvae (G). No LTR punctae form in starved *Syx17* mutants (H), whereas LTR staining is restored in mutants expressing a *Syx17* transgene (I). No LTR dots appear in *VAMP7* mutants (J). (K) Expression of a second, independent *usnp* RNAi transgene also blocks LTR puncta formation. (L–O) Tandem-tagged mCherry-GFP-Atg8a is transported to autolysosomes that appear as mCherry-positive puncta (magenta in L) in control cells of starved larvae. Silencing of *Syx17* (M), *usnp* (N), or *VAMP7* (O) results in the formation of numerous dots positive for both mCherry and GFP (white). Dot plots in L′–O′ show intensity and colocalization profiles of mCherry and GFP dots. Pearson correlation coefficients shown at the top indicate strong colocalization of GFP and mCherry in M′–O′. (P–R) Quantification of data presented in A–C (P), D–F and K (Q), and G–J (R); $n = 10$ for all genotypes. mCh, mCherry. Error bars mark SDs. *, $P < 0.05$; ***, $P < 0.001$. Bar, 20 µm.

recruit usnp, and they mediate fusion of autophagosomes and endo/lysosomes by binding to VAMP7 located in the membranes of the degradative organelles. Endogenous Syx17 was indeed detected in 30.5% (61/200) of endogenous Atg8a-positive autophagosomes in starved animals and also colocalized with 43% (86/200) of GFP-Atg8a dots (Fig. 4, A and B). In contrast, Syx17 essentially did not colocalize with the phagophore marker Atg5 (2.5%, 5/200) or GFP-dLAMP–positive late endosomes and lysosomes (6.8%, 16/236; Fig. 4, C and D). Loss of *Atg2* results in accumulation of stalled phagophores that already contain Atg8 homologues in worms and mammals (Lu et al., 2011; Velikkakath et al., 2012). Accordingly, Atg8a and Syx17 did not colocalize in *Atg2* mutants (2.8%, 9/322; Fig. 4 E). Finally, immuno-EM showed the presence of endogenous Syx17 in the outer membrane of autophagosomes (Fig. 4 F). Thus, Syx17 is recruited to autophagosomes to promote their fusion with late endosomes and lysosomes through its interactions with usnp and VAMP7.

Two papers relying on siRNA depletion of human *STX17* were published while our manuscript was under review (Itakura et al., 2012; Hamasaki et al., 2013). Itakura et al. (2012) found that STX17, SNAP-29, and VAMP8 cooperate to mediate fusion of autophagosomes with late endosomes and lysosomes in mammalian cells. Also, GFP-STX17 localized to the outer membrane of autophagosomes. In contrast, Hamasaki et al. (2013) suggested that no autophagosomes form in *STX17* siRNA–treated

Published May 13, 2013

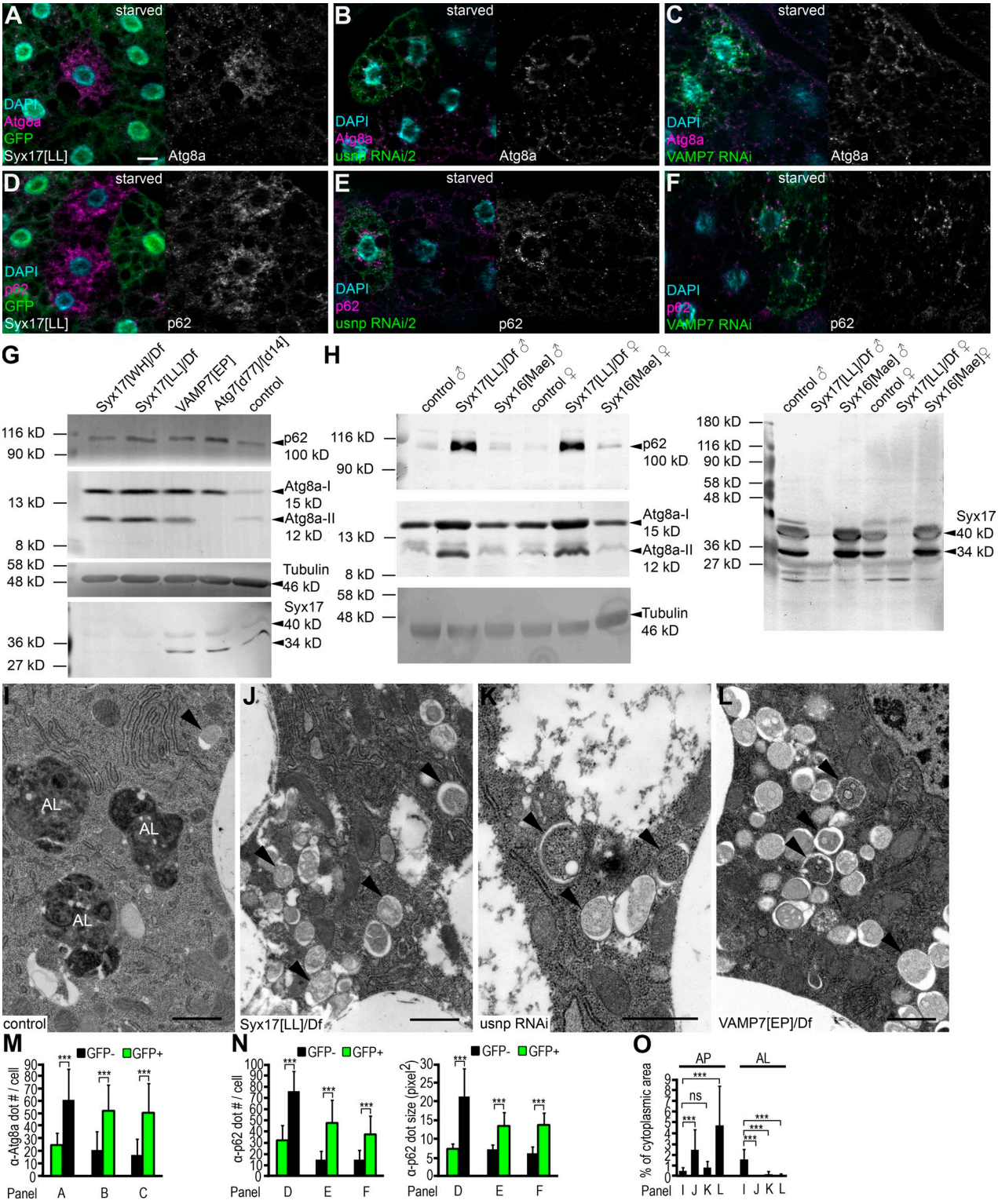

Figure 2. **Autophagosomes accumulate upon loss of *Syx17*, *usnp*, or *VAMP7*.** (A–C) Increased numbers of Atg8a-positive autophagosomes are seen in *Syx17* mutant (A), *usnp* (B), and *VAMP7* (C) RNAi cells in starved larvae. (D–F) p62 aggregates accumulate in *Syx17* mutant (D), *usnp* (E), and *VAMP7* (F) RNAi cells in starved larvae. Note that *Syx17* mutant cells are marked by lack of GFP expression in A and D, whereas RNAi cells express LAMP1-GFP in B, C, E, and F. (G) Western blots show increased autophagosome-associated, lipidated Atg8a-II levels in starved *Syx17* and *VAMP7* mutant larvae compared with controls. Accumulation of p62 in *Syx17* and *VAMP7* mutants is comparable to *Atg7* mutants that are unable to lipidate Atg8a. Both the 34- and 40-kD isoforms of Syx17 disappear in *Syx17[LL]* mutants based on rat anti-Syx17 immunoblots, whereas faint bands are visible in *Syx17[WH]* mutant larvae. (H) Atg8a-II and p62 accumulate in well-fed *Syx17* mutant adults compared with controls or *Syx16* mutants (an additional control). Both Syx17-specific bands are missing from *Syx17* mutant adults. (I–L) Numerous large autolysosomes (AL) and few double-membrane autophagosomes (arrowheads) are visible in ultrastructural images of control fat body cells from starved animals (I). Loss of *Syx17* (J), *usnp* (K), or *VAMP7* (L) function leads to accumulation of autophagosomes and lack of autolysosomes. (M–O) Quantification of data presented in A–C (M), D–F (N), and I–L (O). AP, autophagosome. $n = 10$ for A–F, and $n = 4$ for I–L. Error bars mark SDs. ***, $P < 0.001$. Bars: (A–F) 20 µm; (I–L) 1 µm.

Published May 13, 2013

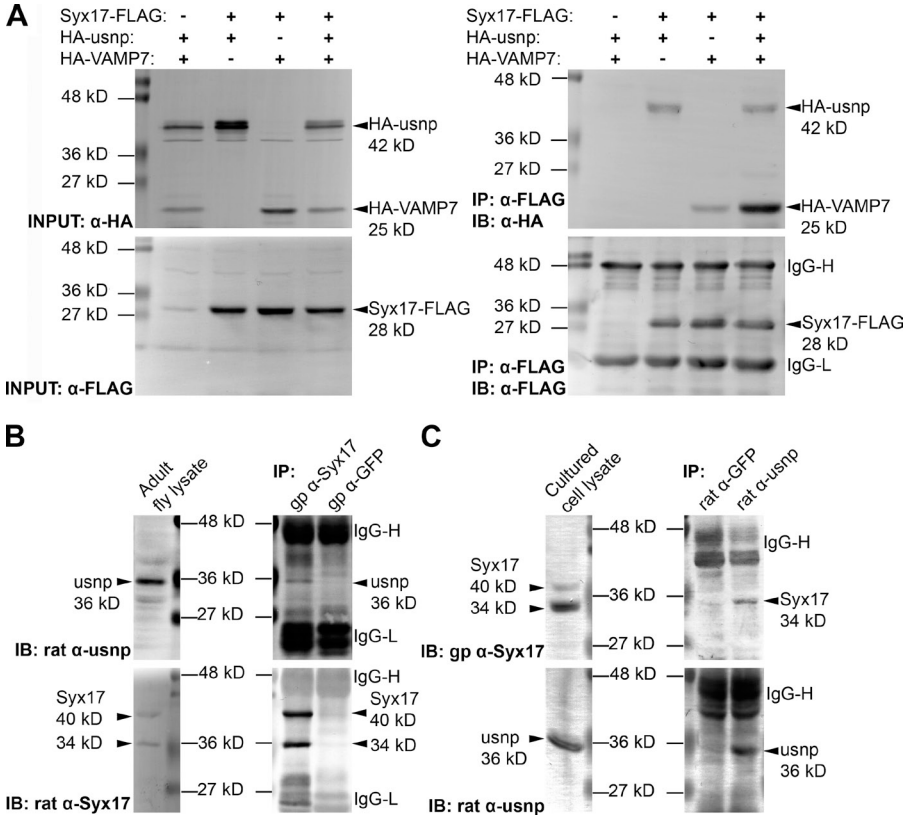

Figure 3. **Syx17 binds to usnp and VAMP7.** (A) Coimmunoprecipitation shows that Syx17-FLAG binds to both HA-usnp and HA-VAMP7 in cultured *Drosophila* cells. Note that usnp facilitates the interaction of overexpressed VAMP7 with Syx17 (both lacking transmembrane domains). (B) Endogenous usnp coimmunoprecipitates with endogenous Syx17. (C) Endogenous Syx17 coimmunoprecipitates with endogenous usnp. gp, guinea pig; IP, immunoprecipitation; IB, immunoblotting.

cells. Our results support the findings of the former work with the exception of VAMP8, but flies appear to have only VAMP7 and lack the closely related VAMP8. According to Itakura et al. (2012), a pool of free cytosolic STX17 may be directly inserted into the outer membrane of autophagosomes. This is likely mediated by its two glycine-rich transmembrane domains and the C-terminal region (Itakura et al., 2012). *Drosophila* Syx17 shows a similar domain structure to human STX17, so it may also be transported to autophagosomes by this pathway (Fig. S2 C).

Depletion of *syntaxin5* was recently shown to cause defects in autophagic protein degradation caused by impaired trafficking of hydrolases from ER to Golgi and thus lysosomes (Renna et al., 2011). Importantly, *syntaxin5* seemed to be dispensable for the fusion of autophagosomes with endosomes and lysosomes, indicating that it functions at a later step during autophagy than Syx17.

Continuous basal autophagy is critical for the homeostasis of quiescent, nondividing cells, such as neurons. We and others reported earlier that autophagy deficiency results in accumulation of protein aggregates and progressive neurodegeneration in flies and mice (Hara et al., 2006; Komatsu et al., 2006; Juhász et al., 2007). *Syx17* mutant adults were viable but unable to fly or climb properly, and all died within 4 d of eclosion (n = 351). We detected large-scale accumulation of Atg8a-positive autophagosomes and p62 aggregates in *Syx17* mutant brains (Fig. 5, A, B, and F). Neurons of well-fed *Syx17* mutant adult flies contained vast numbers of autophagosomes: on average, 20% of total cytoplasm was enclosed within them (Fig. 5, D and G). In contrast, autophagic structures were rarely observed in ultrastructural images of control brains or mutants rescued by transgenic expression of Syx17 (Fig. 5, C, E, and G). Altogether 86% of cells (201/234, n = 4) contained autophagosomes in ultrastructural sections of mutant brains, in contrast with 1% of neurons in control flies (3/270, n = 4) or 2% in rescued flies (6/327, n = 4).

2-d-old *Syx17* mutants performed poorly in a climbing test (Fig. 5 H), an established measure of nervous system function (Juhász et al., 2007). Again, transgenic expression of Syx17 rescued this locomotion defect (Fig. 5 H). We showed earlier that loss of *Atg7* leads to widespread apoptosis in brains of 30-d-old mutant adults (Juhász et al., 2007). On average, 25% of neurons were positive for active caspase 3 in the absence of Syx17 in mutant brains, unlike in similarly aged controls (Fig. S2, D–F). TUNEL assays showed that 20% of mutant cells contained fragmented DNA indicating cell death, whereas practically no TUNEL-positive neurons were identified in control or rescued 2-d-old adult brains (Fig. 5, I–K; and Fig. S2 G, quantification). This seemed specific to neurons, as no TUNEL-positive cells were detected in muscles of mutant adults (Fig. S2, H and I). Transgenic expression of the effector caspase inhibitor p35 in mutant neurons suppressed TUNEL staining (Fig. S2, G and J), but 85% of neurons (202/238, n = 3) still contained autophagosomes in brain sections similar to *Syx17* mutants (Fig. S2 K). The potential contribution of caspase activation to mutant phenotypes was tested in epistasis analyses. Neuron-specific expression of p35 or the pancaspase inhibitor DIAP1 (*Drosophila* inhibitor of apoptosis protein 1) failed to rescue locomotion defects in 2-d-old *Syx17* mutant adults (Fig. 5 H). In addition, although transgenic expression of Syx17 fully rescued the viability of *Syx17* mutant adults (174/175 adults alive on day 4),

Published May 13, 2013

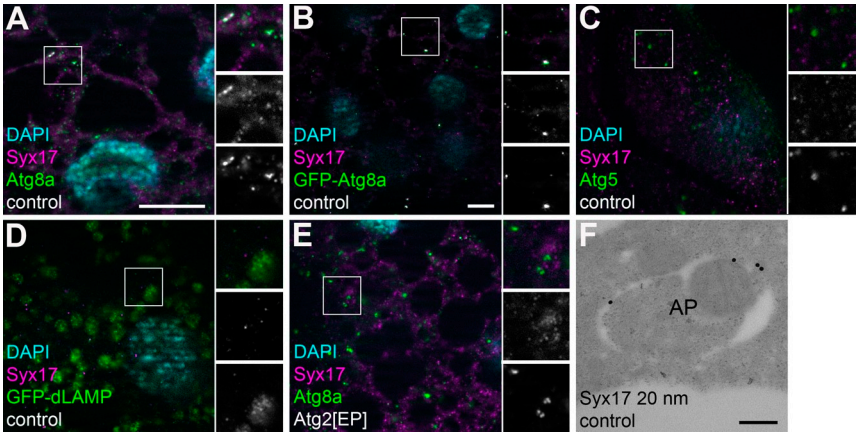

Figure 4. **Syx17 is recruited to completed autophagosomes.** (A and B) Endogenous Syx17 colocalizes with both endogenous (A) and GFP-tagged (B) Atg8a in starved fat body cells. (C and D) No colocalization is observed between Syx17 and the phagophore marker Atg5 (C) or late endosomes and lysosomes, labeled by GFP-dLAMP (D). (E) Syx17 and Atg8a do not colocalize in *Atg2* mutants that accumulate Atg8a-positive stalled phagophores. Insets show merged images (top), Syx17 channels (middle), and relevant green channels (bottom) enlarged from boxed areas in A–E. (F) Immunogold labeling reveals that Syx17 is associated with the outer membrane of autophagosomes (AP). Bars: (A and C–E) 20 µm; (B) 20 µm; (F) 100 nm.

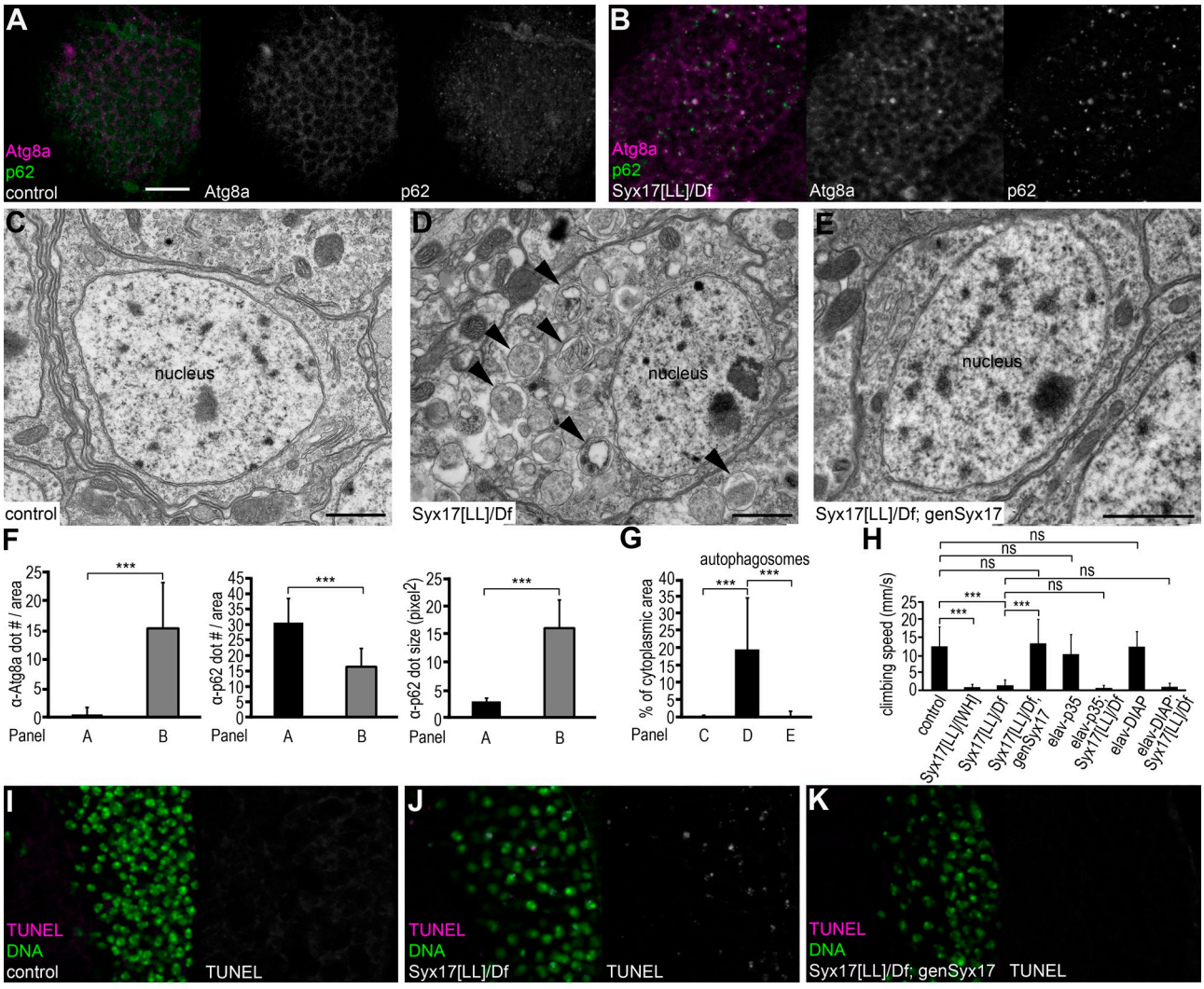

Figure 5. **Impaired autophagosome maturation leads to locomotion defects in 2-d-old adult flies.** (A and B) Atg8a-positive autophagosomes and p62 aggregates accumulate in *Syx17* mutant brains (B) compared with similarly aged controls (A). (C–E) No autophagosomes are found by EM in neurons of control adult flies (C). Large-scale accumulation of autophagosomes (arrowheads) is obvious in *Syx17* mutant neurons (D). Autophagosome accumulation is rescued in *Syx17* mutant neurons by transgenic expression of Syx17 (E). (F and G) Quantification of data presented in A and B (F) and C–E (G); $n = 9$ for A and B, and $n = 4$ for C–E. Error bars mark SDs. ***, $P < 0.001$. (H) *Syx17* mutant adults perform poor compared with controls in climbing tests. Expression of Syx17 in mutants rescues locomotion defects. Neuron-specific expression of caspase inhibitors p35 or DIAP1 have no influence on climbing performance of adult flies, and these do not rescue the defects of *Syx17* mutant adults. $n = 90$ for all genotypes. Error bars mark SDs. ***, $P < 0.001$. (I–K) TUNEL assays reveal apoptotic DNA fragmentation in *Syx17* mutant brains (J) compared with controls (I), which is rescued by expression of Syx17 (K). Bars: (A, B, and I–K) 20 µm; (C–E) 1 µm.

Published May 13, 2013

all mutant flies expressing either p35 or DIAP1 still died within 4 d of eclosion (n = 90 and 105, respectively). These results suggest that neuronal caspase activation may not be a major cause for the locomotion defects and premature death of *Syx17* mutant adult flies.

Collectively, we showed that a complex of SNARE proteins Syx17, usnp, and VAMP7 is required for autophagosome clearance and that autophagosomes gain competence to fuse with late endosomes and lysosomes by recruiting Syx17. The locomotion defects and early death of viable *Syx17* mutants indicate that lysosomal degradation and recycling of sequestered autophagosomal cargo is crucial to maintain organismal health and proper brain functions in *Drosophila*.

Materials and methods

Fly strains and genetics

Flies were maintained on standard yeast/cornmeal/agar media. In climbing tests, a total of 90 adults per genotype were recorded and scored in cohorts of three to six flies, after tapping them down in a plastic graduated cylinder (Juhász et al., 2007). In clonal analyses, RNAi cells were generated spontaneously in larvae carrying hs-Flp; upstream activation sequence (UAS)-Dcr2; Actin>CD2>Gal4 UAS-RNAi (and UAS-GFP or UAS-LAMP1-GFP as a knockdown cell marker), and mutant cell clones (marked by lack of GFP expression) were generated by heat shocking 2–4-h embryos of the genotype hs-Flp; ubi-GFP FRT2A/Syx17[LL] FRT2A in a 38°C water bath for 1 h (Juhász et al., 2007, 2008; Pircs et al., 2012). Expression of mCherry-Atg8a was driven by a fat body–specific r4 promoter in our screen (transgenic flies were provided by T. Neufeld, University of Minnesota, Minneapolis, MN; Pircs et al., 2012). We used the GFP knockin line dLAMP[CPTI001775] (Drosophila Genetic Resource Center) to label lysosomes, w[1118] as control, UAS-GFP-KDEL and Pdi[G00198] as ER reporters (Bloomington Drosophila Stock Center), Atg2[EP3697] (Berry and Baehrecke, 2007), Atg7[d77]/Atg7[d14] (Juhász et al., 2007) mutants, and SNARE loss-of-function strains listed in Table S1. Knockdown of usnp was induced by Actin-Gal4 for Western blots and collagen-Gal4 for EM in L3 stage larvae, and overexpression of UAS-p35 or UAS-DIAP1 in adult neurons was mediated by elav-Gal4 (all obtained from Bloomington Drosophila Stock Center).

Histology and imaging

LTR stainings were performed by incubating dissected L3 stage fat bodies in 100 nM LTR (Invitrogen) for 5 min. For immunofluorescent labeling, bisected larvae were fixed overnight in 3.7% paraformaldehyde at 4°C and blocked in PBS with 0.1% Triton X-100, 0.05% sodium deoxycholate, and 3% goat serum for 3 h followed by overnight incubations with primary and secondary antibodies in blocking buffer at 4°C (Juhász et al., 2008; Pircs et al., 2012). We used chicken anti-GFP (1:1,500; Invitrogen), rabbit anti-Atg5 (1:100; Sigma-Aldrich), rabbit anti-Atg8a (1:500; provided by K. Kohler, Eidgenössische Technische Hochschule Zürich, Zurich, Switzerland; Barth et al., 2011), rabbit anti-p62 (1:2,000; Pircs et al., 2012), rabbit anti–active caspase 3 (1:300; Cell Signaling Technology), rat anti-Atg8a (1:300), and rat anti-Syx17 (1:300; this study) primary and Alexa Fluor 488 anti–chicken, Alexa Fluor 488 anti–rabbit, Alexa Fluor 568 anti–rat, and Alexa Fluor 647 anti–rabbit (all 1:1,500; Invitrogen) secondary antibodies. For TUNEL stainings, adult heads and half-thoraces were fixed in 3.7% paraformaldehyde overnight at 4°C and embedded into paraffin following standard protocols. Sections were processed using In Situ Cell Death Detection Kit, tetramethylrhodamine red (Roche) with SYTOX green DNA stain (Juhász et al., 2007). Images were obtained on a microscope (Axio Imager.M2; Carl Zeiss) equipped with a grid confocal unit (ApoTome.2; Carl Zeiss) at room temperature, using Plan-Neofluar 20×, 0.5 NA (air), 40×, 0.75 NA (air), and 100×, 1.3 NA (oil) objectives, a camera (AxioCam MRm; Carl Zeiss), and AxioVision software (Carl Zeiss). Microscope settings were identical for experiments of the same kind. Primary images were processed in AxioVision and Photoshop (Adobe) to produce final figures. Note that Alexa Fluor 568 or 647 channels are pseudocolored magenta.

Image analysis and statistics

Colocalization of puncta was counted manually on a computer situated in a darkroom, only taking into account overlapping structures with a similar shape and size in relevant fluorescent channels. For statistical analyses, original, unmodified images were imported in ImageJ (National Institutes of Health), and the intensity threshold for the relevant channel was set so that as many dots as possible were selected without the merging of clearly separable adjacent dots. In clonal analyses, mutant or RNAi cells were then manually encircled based on the GFP channel, and the number and size of dots in the relevant channel within that area were recorded. Adjacent control cells were selected randomly from the same image and analyzed. When comparing images from different control and mutant animals, a 300 × 300–pixel area was randomly selected from each image and analyzed as in clonal experiments. Images taken from the number of animals (n) per genotype as indicated in figure legends were evaluated for all experiments. Data were then imported into SPSS Statistics (IBM) and tested for normality of data distribution, and then, p-values were calculated with the appropriate statistical tests: two-tailed, two-sample, unequal variance t test or U test for pairwise comparison of normal or nonnormal distribution data, respectively, and analysis of variance or nonparametric Kruskal-Wallis tests for multiple comparisons of normal or nonnormal distribution data, respectively. For autophagic flux measurements with mCherry-GFP-Atg8a, primary images were imported into ImageJ and analyzed automatically using the colocalization plugin with the intensity correlation tool. Clones from 5–10 animals per genotype were evaluated with similar results, and one representative dot plot is shown in Fig. 1 (L′–O′) for each.

Molecular cloning and generation of polyclonal antibodies

The genomic region containing *Drosophila* Syx17 was amplified using primers 5′-GGCGCGCCGCATGCGGCCGCTTAGACGTAAGCGCACCACCGC-3′ and 5′-GCATGCTAGCGGCCGCGTGACCAACGAGAACACGGGC-3′ and cloned into pCasper5 as an SphI fragment. Transgenic flies genSyx17 were generated following standard procedures (BestGene, Inc.). Syx17 coding sequences were amplified by PCR using primers 5′-ATGACGCGCGATGAGAAACTGCC-3′ and 5′-ATCCTTCTGGCTTCTCTTTTAGCTCCAGTCTCTC-3′, phosphorylated, blunt cloned into XmnI–EcoRV-digested dephosphorylated pENTR1A (Invitrogen), and subsequently recombined into pDEST17 (Invitrogen). N-terminally His-tagged protein was expressed in the *Escherichia coli* Rosetta strain (EMD Millipore) and purified using Ni-agarose beads (QIAGEN). Recombinant protein was used to immunize rats and guinea pigs following standard procedures with Freund's adjuvants (Sigma-Aldrich). Syx17 pENTR1A was recombined into pTWF (Drosophila Genomics Resource Center) to yield UAS-Syx17-FLAG, in which 3×FLAG replaces the two transmembrane domains and the extreme C-terminal region of Syx17. usnp and VAMP7 coding sequences were amplified using primers 5′-GTAGCGGCCGCGGGTACCGGAATGGCCCATAACTACCTGCAGC-3′/5′-TATGGTACCGCGGCCGCTACTTCTTCAGAAGCTTGCTCATGTCC-3′ and 5′-GTAGCGGCCGCGGGTACCGGACCGATACTATATAGTGTGATATCGCGGG-3′/5′-ATATGGTACCGCGGCCGCTAGACGCGGATGTTCTTCCAAAA-3′, respectively, and cloned into pUAST-3×HA to generate UAS-HA-usnp and UAS-HA-VAMP7. Note that the transmembrane domain is removed from tagged VAMP7. The aforementioned primers were used to blunt clone usnp coding sequences into pENTR1A followed by recombination of the resulting entry clone into pDEST17, expression and purification of the recombinant protein, and immunization of rats as for Syx17.

Cell culture and coimmunoprecipitations

Embryonic hemocyte-derived D.Mel-2 cells were maintained in Express-Five Serum-Free medium (Invitrogen) and transfected with UAS constructs and metallothionein-Gal4 plasmid using TransIT-2020 reagent (Mirus Bio LLC). 48 h later, protein expression was induced by adding 1 mM $CuSO_4$ for overnight incubation. Cultured cells were collected, washed twice in PBS, lysed on ice in lysis buffer (0.5% Triton X-100, 150 mM NaCl, 1 mM EDTA, and 20 mM Tris-HCl, pH 7.5) containing complete protease and phosphatase inhibitor cocktails (Sigma-Aldrich), and spun for 10 min at 10,000 *g* in a centrifuge (5430R; Eppendorf) at 4°C followed by the addition of anti-FLAG slurry (Sigma-Aldrich) to the cleared supernatant. After incubation at 4°C for 2 h, beads were collected by centrifugation at 5,000 *g* for 30 s at 4°C followed by extensive washes in lysis buffer and finally boiling in 30 µl Laemmli sample buffer. Coimmunoprecipitations were repeated using a different DNA clone for all constructs, with similar results. For endogenous interaction experiments, either 100 mg of adult flies was starved for 2 h or 150 mg of cultured cells was washed for 2 × 10 min in PBS and homogenized for 2 × 10 s on ice in 1 ml lysis buffer containing 1% Triton X-100, using an homogenizer (Ultra-Turret T10; IKA) equipped with a disperser (S10N-5G; IKA). Lysates were cleared by centrifugation at 30,130 *g* for 10 min at 4°C (adult supernatants were spun once more to completely

get rid of fat and unbroken cuticle pieces) followed by incubation with 3 µl rat anti-usnp (this study) or anti-GFP (Pircs et al., 2012), or guinea pig anti-Syx17 (this study) or anti-GFP (raised in collaboration with J. Mihály and I. Andó, Biological Research Center, Szeged, Hungary) antisera for 2 h at 4°C. Antibody–antigen complexes were collected by addition of 20 µl protein A (for guinea pig sera) or protein G (for rat sera) agarose 50% slurry for 1 h at 4°C and processed for Western blots as in co-overexpression experiments. Immunoprecipitations were performed from both cultured cells and adult flies, and representative examples are shown.

Transmission EM and immuno-EM

Dissected tissues were fixed in 3.2% paraformaldehyde, 0.5% glutaraldehyde, 1% sucrose, and 0.028% $CaCl_2$ in 0.1 N sodium cacodylate, pH 7.4, overnight at 4°C, postfixed in 0.5% osmium tetroxide for 1 h, and embedded into Durcupan (Fluka) according to the manufacturer's recommendations (Juhász et al., 2007, 2008). 70-nm sections were stained in Reynold's lead citrate and viewed on a transmission electron microscope (JEM-1011; JEOL) equipped with camera (Morada; Olympus) and iTEM software (Olympus). A total of 17–29 randomly taken 10,000× magnification images of sections from four animals were evaluated per genotype by manually encircling relevant structures in Photoshop and calculating their percentage of area relative to total cytoplasm. P-values were calculated as described in Image analysis and statistics. For immuno-EM, samples were fixed as for conventional EM and embedded in London Resin white resin (Sigma-Aldrich) without postfixation. 90-nm sections were cut and incubated with rat anti-Syx17 (1:30) in PBS with 3% milk overnight at 4°C followed by biotin-conjugated anti–rat (1:100; Jackson ImmunoResearch Laboratories, Inc.) for 1 h in PBS with 1.5% milk at 25°C and anti-biotin conjugated to 20-nm gold for 5 h in TBS with 1.5% milk and 0.25% Tween 20 at 4°C (1:100; British Biocell; Juhász et al., 2007, 2008).

Western blots

Equal amounts of proteins per sample were separated by denaturing SDS-PAGE and processed for Western blots as previously described (Juhász et al., 2007; Pircs et al., 2012). Mouse anti-tubulin (1:1,000; AA4.3-s; Developmental Studies Hybridoma Bank), mouse anti-FLAG (1:2,000; M2; Sigma-Aldrich), rabbit anti-HA (1:2,000; Sigma-Aldrich), rabbit anti-p62 (1:8,000; Pircs et al., 2012), rabbit anti-Atg8a (1:5,000), rat anti-Syx17 (1:5,000; this study), guinea pig anti-Syx17 (1:5,000; this study), rat anti-usnp (1:3,000; this study) primary and alkaline phosphatase–conjugated anti–guinea pig, anti–rat (1:5,000; Sigma-Aldrich), anti–rabbit, and anti–mouse (1:5,000; EMD Millipore) secondary antibodies were used in TBS, pH 7.4, with 0.1% Tween 20 and 0.25% casein followed by colorimetric detection with nitro-blue tetrazolium–5-bromo-4-chloro-3-indolyl phosphate (Sigma-Aldrich).

Online supplemental material

Fig. S1 shows that *Syx17*, *usnp*, and *VAMP7* are required for developmental and basal autophagy. Fig. S2 shows additional Syx17 localization, sequence alignment, and interaction data. Table S1 lists *Drosophila* homologues of human and yeast SNARE proteins, RNAi and mutant lines for these genes used in this study, and results of our small-scale RNAi screen. Online supplemental material is available at http://www.jcb.org/cgi/content/full/jcb.201211160/DC1. Additional data are available in the JCB DataViewer at http://dx.doi.org/10.1083/jcb.201211160.dv.

We thank Sarolta Pálfia, Zsófia Kováts, Eszter Papp, and Eszter Vágó for technical assistance, public repositories, and colleagues listed in the Materials and methods section for reagents,

We thank the Wellcome Trust (087518/Z/08/Z), the Hungarian Scientific Research Fund (K83509), and the Hungarian Academy of Sciences (BO/00552/11) for support.

Submitted: 28 November 2012
Accepted: 11 April 2013

References

Atlashkin, V., V. Kreykenbohm, E.L. Eskelinen, D. Wenzel, A. Fayyazi, and G. Fischer von Mollard. 2003. Deletion of the SNARE vti1b in mice results in the loss of a single SNARE partner, syntaxin 8. *Mol. Cell. Biol.* 23:5198–5207. http://dx.doi.org/10.1128/MCB.23.15.5198-5207.2003

Axe, E.L., S.A. Walker, M. Manifava, P. Chandra, H.L. Roderick, A. Habermann, G. Griffiths, and N.T. Ktistakis. 2008. Autophagosome formation from membrane compartments enriched in phosphatidylinositol 3-phosphate and dynamically connected to the endoplasmic reticulum. *J. Cell Biol.* 182:685–701. http://dx.doi.org/10.1083/jcb.200803137

Barth, J.M., J. Szabad, E. Hafen, and K. Köhler. 2011. Autophagy in *Drosophila* ovaries is induced by starvation and is required for oogenesis. *Cell Death Differ.* 18:915–924. http://dx.doi.org/10.1038/cdd.2010.157

Berry, D.L., and E.H. Baehrecke. 2007. Growth arrest and autophagy are required for salivary gland cell degradation in *Drosophila*. *Cell*. 131:1137–1148. http://dx.doi.org/10.1016/j.cell.2007.10.048

Bjørkøy, G., T. Lamark, S. Pankiv, A. Øvervatn, A. Brech, and T. Johansen. 2009. Monitoring autophagic degradation of p62/SQSTM1. *Methods Enzymol.* 452:181–197. http://dx.doi.org/10.1016/S0076-6879(08)03612-4

Dilcher, M., B. Köhler, and G.F. von Mollard. 2001. Genetic interactions with the yeast Q-SNARE VTI1 reveal novel functions for the R-SNARE YKT6. *J. Biol. Chem.* 276:34537–34544. http://dx.doi.org/10.1074/jbc.M101551200

Fader, C.M., D.G. Sánchez, M.B. Mestre, and M.I. Colombo. 2009. TI-VAMP/VAMP7 and VAMP3/cellubrevin: two v-SNARE proteins involved in specific steps of the autophagy/multivesicular body pathways. *Biochim. Biophys. Acta.* 1793:1901–1916. http://dx.doi.org/10.1016/j.bbamcr.2009.09.011

Filimonenko, M., S. Stuffers, C. Raiborg, A. Yamamoto, L. Malerød, E.M. Fisher, A. Isaacs, A. Brech, H. Stenmark, and A. Simonsen. 2007. Functional multivesicular bodies are required for autophagic clearance of protein aggregates associated with neurodegenerative disease. *J. Cell Biol.* 179:485–500. http://dx.doi.org/10.1083/jcb.200702115

Furuta, N., N. Fujita, T. Noda, T. Yoshimori, and A. Amano. 2010. Combinational soluble N-ethylmaleimide-sensitive factor attachment protein receptor proteins VAMP8 and Vti1b mediate fusion of antimicrobial and canonical autophagosomes with lysosomes. *Mol. Biol. Cell*. 21:1001–1010. http://dx.doi.org/10.1091/mbc.E09-08-0693

Hamasaki, M., N. Furuta, A. Matsuda, A. Nezu, A. Yamamoto, N. Fujita, H. Oomori, T. Noda, T. Haraguchi, Y. Hiraoka, et al. 2013. Autophagosomes form at ER-mitochondria contact sites. *Nature*. 495:389–393. http://dx.doi.org/10.1038/nature11910

Hara, T., K. Nakamura, M. Matsui, A. Yamamoto, Y. Nakahara, R. Suzuki-Migishima, M. Yokoyama, K. Mishima, I. Saito, H. Okano, and N. Mizushima. 2006. Suppression of basal autophagy in neural cells causes neurodegenerative disease in mice. *Nature*. 441:885–889. http://dx.doi.org/10.1038/nature04724

Hong, W. 2005. SNAREs and traffic. *Biochim. Biophys. Acta*. 1744:120–144. http://dx.doi.org/10.1016/j.bbamcr.2005.03.014

Ishihara, N., M. Hamasaki, S. Yokota, K. Suzuki, Y. Kamada, A. Kihara, T. Yoshimori, T. Noda, and Y. Ohsumi. 2001. Autophagosome requires specific early Sec proteins for its formation and NSF/SNARE for vacuolar fusion. *Mol. Biol. Cell*. 12:3690–3702.

Itakura, E., C. Kishi-Itakura, and N. Mizushima. 2012. The hairpin-type tail-anchored SNARE syntaxin 17 targets to autophagosomes for fusion with endosomes/lysosomes. *Cell*. 151:1256–1269. http://dx.doi.org/10.1016/j.cell.2012.11.001

Juhász, G., B. Erdi, M. Sass, and T.P. Neufeld. 2007. Atg7-dependent autophagy promotes neuronal health, stress tolerance, and longevity but is dispensable for metamorphosis in *Drosophila*. *Genes Dev.* 21:3061–3066. http://dx.doi.org/10.1101/gad.1600707

Juhász, G., J.H. Hill, Y. Yan, M. Sass, E.H. Baehrecke, J.M. Backer, and T.P. Neufeld. 2008. The class III PI(3)K Vps34 promotes autophagy and endocytosis but not TOR signaling in *Drosophila*. *J. Cell Biol.* 181:655–666. http://dx.doi.org/10.1083/jcb.200712051

Kimura, S., T. Noda, and T. Yoshimori. 2007. Dissection of the autophagosome maturation process by a novel reporter protein, tandem fluorescent-tagged LC3. *Autophagy*. 3:452–460.

Komatsu, M., S. Waguri, T. Chiba, S. Murata, J. Iwata, I. Tanida, T. Ueno, M. Koike, Y. Uchiyama, E. Kominami, and K. Tanaka. 2006. Loss of autophagy in the central nervous system causes neurodegeneration in mice. *Nature*. 441:880–884. http://dx.doi.org/10.1038/nature04723

Lu, Q., P. Yang, X. Huang, W. Hu, B. Guo, F. Wu, L. Lin, A.L. Kovács, L. Yu, and H. Zhang. 2011. The WD40 repeat PtdIns(3)P-binding protein EPG-6 regulates progression of omegasomes to autophagosomes. *Dev. Cell*. 21:343–357. http://dx.doi.org/10.1016/j.devcel.2011.06.024

Mizushima, N., B. Levine, A.M. Cuervo, and D.J. Klionsky. 2008. Autophagy fights disease through cellular self-digestion. *Nature*. 451:1069–1075. http://dx.doi.org/10.1038/nature06639

Moreau, K., B. Ravikumar, M. Renna, C. Puri, and D.C. Rubinsztein. 2011. Autophagosome precursor maturation requires homotypic fusion. *Cell*. 146:303–317. http://dx.doi.org/10.1016/j.cell.2011.06.023

Nair, U., A. Jotwani, J. Geng, N. Gammoh, D. Richerson, W.L. Yen, J. Griffith, S. Nag, K. Wang, T. Moss, et al. 2011. SNARE proteins are required for macroautophagy. *Cell*. 146:290–302. http://dx.doi.org/10.1016/j.cell.2011.06.022

Ohashi, Y., and S. Munro. 2010. Membrane delivery to the yeast autophagosome from the Golgi-endosomal system. *Mol. Biol. Cell*. 21:3998–4008. http://dx.doi.org/10.1091/mbc.E10-05-0457

Pircs, K., P. Nagy, A. Varga, Z. Venkei, B. Erdi, K. Hegedus, and G. Juhasz. 2012. Advantages and limitations of different p62-based assays for estimating autophagic activity in *Drosophila*. *PLoS ONE*. 7:e44214. http://dx.doi.org/10.1371/journal.pone.0044214

Renna, M., C. Schaffner, A.R. Winslow, F.M. Menzies, A.A. Peden, R.A. Floto, and D.C. Rubinsztein. 2011. Autophagic substrate clearance requires activity of the syntaxin-5 SNARE complex. *J. Cell Sci.* 124:469–482. http://dx.doi.org/10.1242/jcs.076489

Rusten, T.E., T. Vaccari, K. Lindmo, L.M. Rodahl, I.P. Nezis, C. Sem-Jacobsen, F. Wendler, J.P. Vincent, A. Brech, D. Bilder, and H. Stenmark. 2007. ESCRTs and Fab1 regulate distinct steps of autophagy. *Curr. Biol.* 17:1817–1825. http://dx.doi.org/10.1016/j.cub.2007.09.032

Simonsen, A., R.C. Cumming, A. Brech, P. Isakson, D.R. Schubert, and K.D. Finley. 2008. Promoting basal levels of autophagy in the nervous system enhances longevity and oxidant resistance in adult *Drosophila*. *Autophagy*. 4:176–184.

Steegmaier, M., B. Yang, J.S. Yoo, B. Huang, M. Shen, S. Yu, Y. Luo, and R.H. Scheller. 1998. Three novel proteins of the syntaxin/SNAP-25 family. *J. Biol. Chem.* 273:34171–34179. http://dx.doi.org/10.1074/jbc.273.51.34171

Tooze, S.A., and T. Yoshimori. 2010. The origin of the autophagosomal membrane. *Nat. Cell Biol.* 12:831–835. http://dx.doi.org/10.1038/ncb0910-831

Velikkakath, A.K., T. Nishimura, E. Oita, N. Ishihara, and N. Mizushima. 2012. Mammalian Atg2 proteins are essential for autophagosome formation and important for regulation of size and distribution of lipid droplets. *Mol. Biol. Cell*. 23:896–909. http://dx.doi.org/10.1091/mbc.E11-09-0785

Published May 13, 2013

Takáts et al., http://www.jcb.org/cgi/content/full/jcb.201211160/DC1

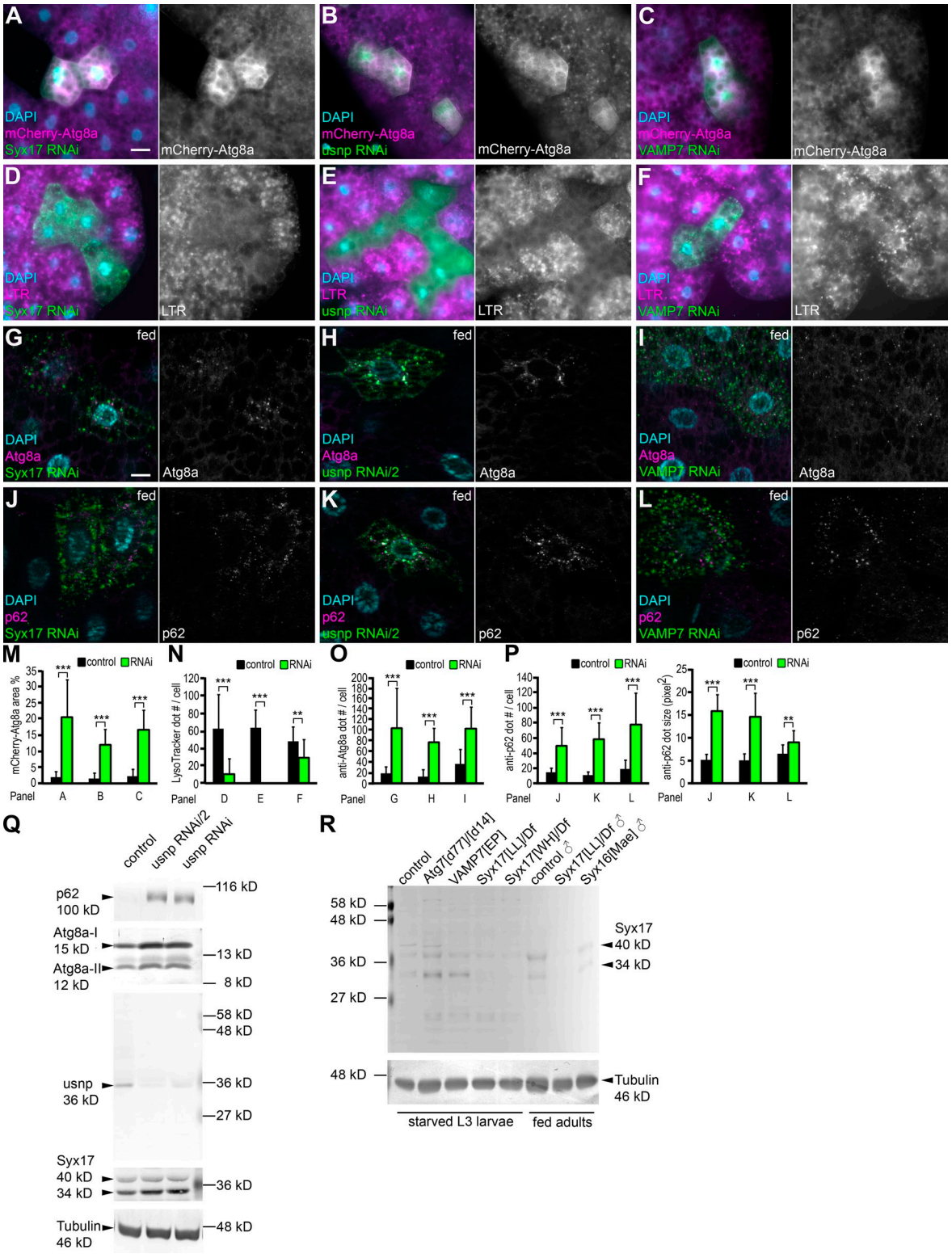

Figure S1. ***Syx17, usnp,* and *VAMP7* are required for developmental and basal autophagy.** (A–C) Knockdown of *Syx17* (A), *usnp* (B), or *VAMP7* (C) in GFP-marked fat body cells results in large-scale accumulation of small mCherry-Atg8a dots in wandering L3 stage larvae. (D–F) *Syx17* (D), *usnp* (E), or *VAMP7* (F) RNAi blocks LysoTracker dot formation in wandering animals. (G–I) Atg8a-positive autophagosomes accumulate in *Syx17* (G), *usnp* (H), and *VAMP7* (I) RNAi cells marked by LAMP1-GFP compared with adjacent control fat body cells in well-fed larvae. (J–L) Accumulation of p62 aggregates is obvious in *Syx17* (J)-, *usnp* (K)-, and *VAMP7* (L)-depleted fat cells in well-fed larvae. (M–P) Quantification of data shown in A–C (M), D–F (N), G–I (O), and J–L (P). $n = 10$ for all genotypes. Error bars mark SDs. **, $P < 0.01$; ***, $P < 0.001$. (Q) Systemic RNAi silencing of *usnp* mediated by *Actin-Gal4* results in accumulation of p62 and Atg8a-II in Western blots of L3 stage larval lysates. Anti-usnp blot reveals that usnp levels are strongly decreased in *usnp* RNAi animals, whereas Syx17 expression is largely unaffected. (R) Western blot analysis of larval and adult samples shows the specificity of guinea pig anti-Syx17 antisera. Bars: (A for A–F) 40 µm; (G for G–L) 20 µm.

Published May 13, 2013

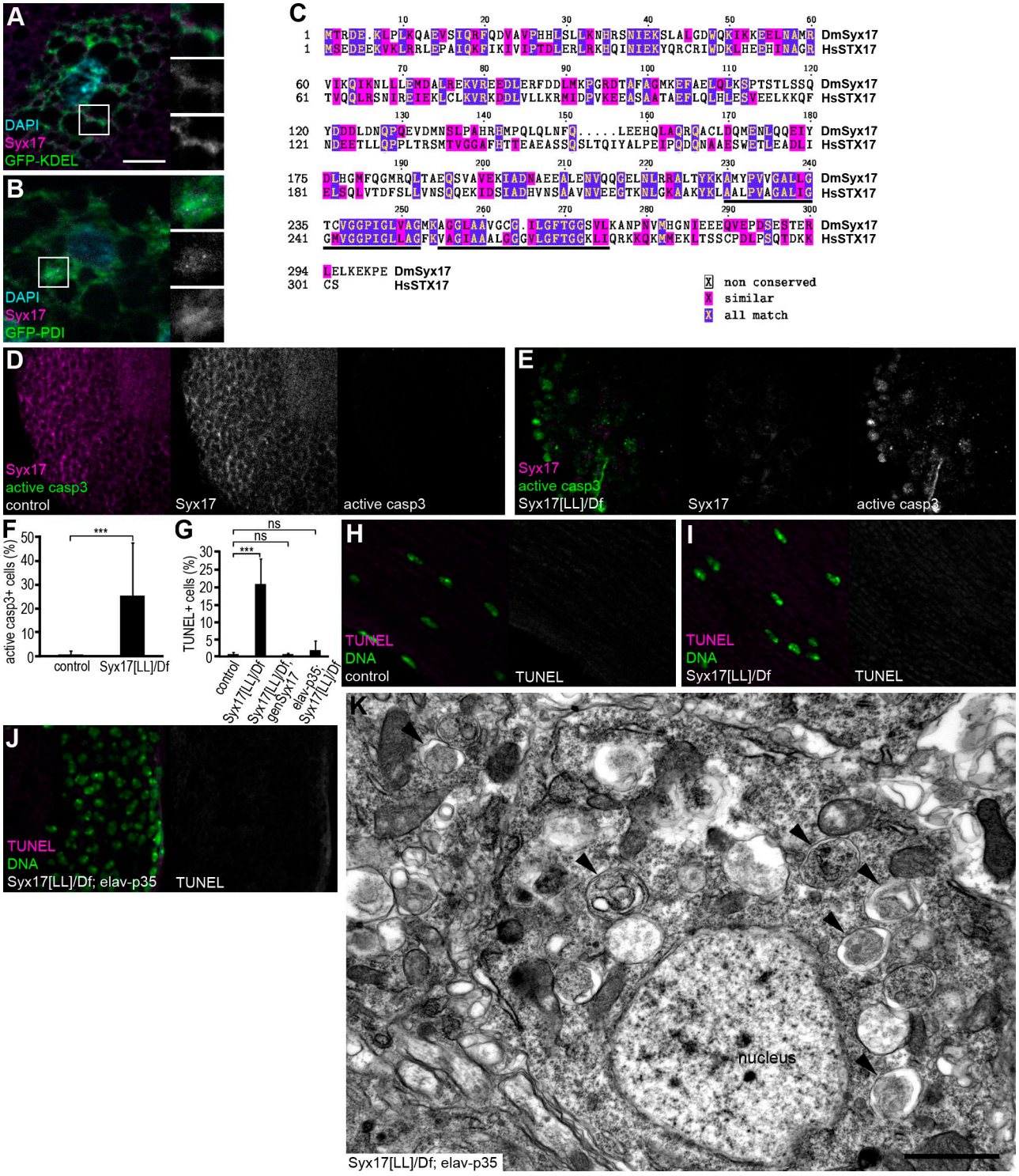

Figure S2. **Additional Syx17 data.** (A and B) Endogenous Syx17 localizes to the region of the ER, marked by GFP-KDEL (A) and GFP–protein disulphide isomerase (B). Insets show merged images (top), Syx17 channels (middle), and relevant green channels (bottom) enlarged from boxed areas in A and B. (C) CLUSTALW alignment of *Drosophila* Syx17 and human STX17. Predicted conserved transmembrane domains are underlined. (D and E) No cleaved caspase 3 labeling is detected in brains of control flies (D). Numerous cells are marked by active caspase 3 immunoreactivity, whereas no specific anti-Syx17 staining is detected in *Syx17* mutant brains (E). (F and G) Quantification of data shown in D and E (F) and J (this figure) and Fig. 5 (I–K) (G). $n = 8$ for all genotypes summarized in panels F and G. Error bars mark SDs. ***, $P < 0.001$. (H and I) TUNEL labeling is almost never seen in adult flight muscles of 2-d-old control animals (H; 2/342 muscle cell nuclei were positive) or in muscles of *Syx17* mutant animals (I; 4/611 nuclei were positive). $n = 3$ for both genotypes. (J) TUNEL staining is suppressed by neuron-specific expression of p35 in 2-d-old *Syx17* mutant adult brains. (K) Autophagosomes (marked by arrowheads) accumulate in brains of 2-d-old *Syx17* mutant adults that express the caspase inhibitor p35 in neurons. Bars: (A for A, B, D, E, and H–J) 20 µm; (K) 1 µm.

Published May 13, 2013

Table S1. **List of *Drosophila* homologues of human and yeast SNARE proteins, RNAi and mutant lines for these genes used in this study, and the results of our small-scale RNAi screen**

Human	Yeast	*Drosophila*	CG number	Strains used	Referred to as	Source	mCherry-Atg8a RNAi phenotype
Syntaxin1	Sso1p/Sso2p	Syntaxin1A	CG31136	JF01829		BDSC/TRiP	No effect
				33112		VDRC	No effect
Syntaxin2							
Syntaxin3							
Syntaxin4		Syntaxin4	CG2715	102466		VDRC	No effect
Syntaxin5	Sed5p	Syntaxin5	CG4214	108928		VDRC	Enhancement
Syntaxin6	Tlg1p	Syntaxin6	CG7736	104795		VDRC	No effect
Syntaxin7	Pep12p	Avalanche/ Syntaxin7	CG5081	107264		VDRC	Suppression
				JF02436		BDSC/TRiP	Suppression
Syntaxin8	Syn8p	Syntaxin8	CG4109	107014		VDRC	No effect
Syntaxin10							
Syntaxin11							
Syntaxin12		Syntaxin13	CG11278	102432		VDRC	No effect
Syntaxin16	Tlg2p	Syntaxin16	CG1467	109504		VDRC	No effect
				JF01924		BDSC/TRiP	No effect
				P{Mae-UAS.6.11}G1176	Syx16[Mae]	BDSC	
Syntaxin17		Syntaxin17	CG7452	JF01937	Syx17 RNAi	BDSC/TRiP	Small perinuclear dots
				PBac{WH}Syx17[f03584]	Syx17[WH]	Harvard Collection	
				PBac{SAstop DsRed}LL06330	Syx17[LL]	DGRC	
				Df(3L)Exel8098	Syx17 Df	BDSC	
Syntaxin18	Ufe1p	Syntaxin18	CG13626	105113		VDRC	Enhancement
SNAP-23	Sec9p	SNAP-25	CG40452	JF02615		BDSC/TRiP	No effect
SNAP-25	Spo20p	SNAP-24	CG9474	108209		VDRC	No effect
SNAP-29		ubisnap	CG11173	JF01883	usnp RNAi	BDSC/TRiP	Small perinuclear dots
				11173R-2	usnp RNAi/2	NIG-Fly	Small perinuclear dots
VAMP1	Snc1p/Snc2p	n-synaptobrevin	CG17248	JF03417		BDSC/TRiP	No effect
VAMP2		Synaptobrevin	CG12210	102922		VDRC	No effect
VAMP3							
VAMP4							
VAMP5							
VAMP7		VAMP7	CG1599	1599R-1	VAMP7 RNAi	NIG-Fly	Small perinuclear dots
				P{EP}CG1599[G7738]	VAMP7[EP]	BDSC	
				Df(2R)BSC132	VAMP7 Df	BDSC	
VAMP8							
Ykt6	Ykt6p	Ykt6	CG1515	105648		VDRC	Enhancement
Sec22a							
Sec22b	Sec22p	Sec22a	CG7359	100766		VDRC	No effect
Sec22c							
Bet1	Bet1p	Bet1	CG14084	8420		VDRC	Suppression
GS15	Sft1p						
GS27	Bos1p	membrin	CG4780	109404		VDRC	No effect
GS28	Gos1p	Gos28	CG7700	100289		VDRC	No effect
Vti1a	Vti1p	Vti1	CG3279	45725		VDRC	No effect
				109819		VDRC	No effect
Vti1b			CG44009				
Slt1	Slt1p/Use1p	Use1	CG14181	100019		VDRC	No effect
Sec20	Sec20p	Sec20	CG2023	100264		VDRC	No effect

VDRC, Vienna Drosophila RNAi Center; BDSC, Bloomington Drosophila Stock Center; TRiP, Transgenic RNAi Project; DGRC, Drosophila Genetic Resource Center; NIG-Fly, National Institutes of Genetics fly stocks.